Electron doping evolution of the neutron spin resonance in NaFe$_{1-x}$Co$_x$As

Chenglin Zhang,[1] Weicheng Lv,[1] Guotai Tan,[2] Yu Song,[1] Scott V. Carr,[1] Songxue Chi,[3] M. Matsuda,[3] A. D. Christianson,[3]
J. A. Fernandez-Baca,[3,4] L. W. Harriger,[5] and Pengcheng Dai[1,2,*]

[1]*Department of Physics and Astronomy, Rice University, Houston, Texas 77005, USA*
[2]*Department of Physics, Beijing Normal University, Beijing 100875, China*
[3]*Quantum Condensed Matter Division, Oak Ridge National Laboratory, Oak Ridge, Tennessee 37831, USA*
[4]*Department of Physics and Astronomy, The University of Tennessee, Knoxville, Tennessee 37996, USA*
[5]*NIST Center for Neutron Research, National Institute of Standards and Technology, Gaithersburg, Maryland 20899, USA*
(Received 4 May 2015; revised manuscript received 24 April 2016; published 31 May 2016)

Neutron spin resonance, a collective magnetic excitation coupled to superconductivity, is one of the most prominent features shared by a broad family of unconventional superconductors including copper oxides, iron pnictides, and heavy fermions. In this paper, we study the doping evolution of the resonances in NaFe$_{1-x}$Co$_x$As covering the entire superconducting dome. For the underdoped compositions, two resonance modes coexist. As doping increases, the low-energy resonance gradually loses its spectral weight to the high-energy one but remains at the same energy. By contrast, in the overdoped regime we only find one single resonance, which acquires a broader width in both energy and momentum but retains approximately the same peak position even when T_c drops by nearly a half compared to optimal doping. These results suggest that the energy of the resonance in electron overdoped NaFe$_{1-x}$Co$_x$As is neither simply proportional to T_c nor the superconducting gap but is controlled by the multiorbital character of the system and doped impurity scattering effect.

I. INTRODUCTION

Although the microscopic origin of superconductivity remains unresolved nearly 30 years after the discovery of high-transition temperature (high-T_c) copper oxides [1], it is generally believed that spin fluctuation mediated electron pairing is a common thread for unconventional superconductors including copper oxide, iron-based, and heavy-fermion superconductors [2,3]. Regardless of the dramatic differences in the ground states of their parent compounds and the microscopic origins of magnetism in different families of unconventional superconductors, inelastic neutron scattering experiments have revealed that superconductivity induces a collective magnetic excitation, termed neutron spin resonance, near the antiferromagnetic (AF) ordering wave vector of their parent compounds [4–8]. Experimentally, the resonance occurs at an energy E_r and enhances dramatically below T_c like the superconducting order parameter. In the Fermi surface nesting (itinerant electron) picture [5], the resonance is a spin-exciton mode in the particle-hole channel. If the superconducting order parameter has a sign change below T_c, the dynamic spin susceptibility will develop a pole, namely the resonance, at an energy E_r below the particle-hole continuum 2Δ (where Δ is the superconducting gap) [5]. In the case of iron pnictide superconductor NaFe$_{1-x}$Co$_x$As with hole and electron Fermi surfaces at Γ and M points, respectively [Figs. 1(a) and 1(e)–1(g)] [9–16], the resonance arises from quasiparticle excitations between the sign-reversed hole and electron Fermi surfaces and occurs at an energy below the sum of their superconducting gap energies ($E_r \leqslant \Delta_h + \Delta_e = 2\Delta$, where Δ_h and Δ_e are superconducting gaps at hole and electron Fermi surfaces, respectively) [Figs. 1(b)–1(d)] [17,18]. Although T_c differs dramatically for copper oxide, iron-

based, and heavy-fermion superconductors, the resonance energy E_r is approximately related to T_c via $E_r/k_B T_c \approx$ 4−6 or the superconducting gap energy Δ via $E_r/2\Delta =$ 0.64 ($2\Delta/k_B T_c = A + B T_c$, where A and B are constants.) [19–21]. While these results suggest that the resonance may be a common thread for unconventional superconductors [2], most of the inelastic neutron scattering measurements on the resonance in iron pnictides are focused on underdoped and optimally doped samples with few experiments on overdoped regime of the phase diagram [20].

In this paper, we report systematic inelastic neutron scattering studies of the resonance in iron pnictide superconductors NaFe$_{1-x}$Co$_x$As for Co compositions throughout the entire superconducting dome [22–26]. In previous work on electron underdoped NaFe$_{0.985}$Co$_{0.015}$As where static AF order coexists with superconductivity ($T_N = 30$ K, and $T_c = 15$ K), we find a dispersive sharp resonance near $E_{r1} = 3.25$ meV and a broad dispersionless mode at $E_{r2} = 6$ meV at the AF ordering wave vector $\mathbf{Q}_{AF}$ [12,27]. Upon moving to electron overdoped NaFe$_{0.955}$Co$_{0.045}$As without static AF order ($T_c = 20$ K), there is only one sharp resonance at $E_r = 7$ meV [28]. By carrying out systematic measurements on NaFe$_{1-x}$Co$_x$As with nominal Co doping of $x = 0.012, 0.0135, 0.0175, 0.025, 0.08$ [Fig. 1(a)], we establish the electron-doping evolution of the resonance throughout the superconducting phase. In the underdoped regime, we confirm the earlier results showing the presence of double resonance peaks at E_{r1} and E_{r2} as shown in Fig. 1(b). As doping increases, E_{r1} stays almost the same value while E_{r2} moves to higher energies. At optimal doping and in slightly overdoped samples, the low-energy resonance disappears and only a single sharp resonance occurs at $E_{r2} = 7$ meV [Fig. 1(c)]. For heavily overdoped $x = 0.08$, the resonance becomes much broader in energy but retains its peak position [Fig. 1(d)]. These results indicate that the resonance energy in the electron overdoped regime is neither directly associated with T_c via the empirical relation $E_r/k_B T_c = 4 \sim 6$
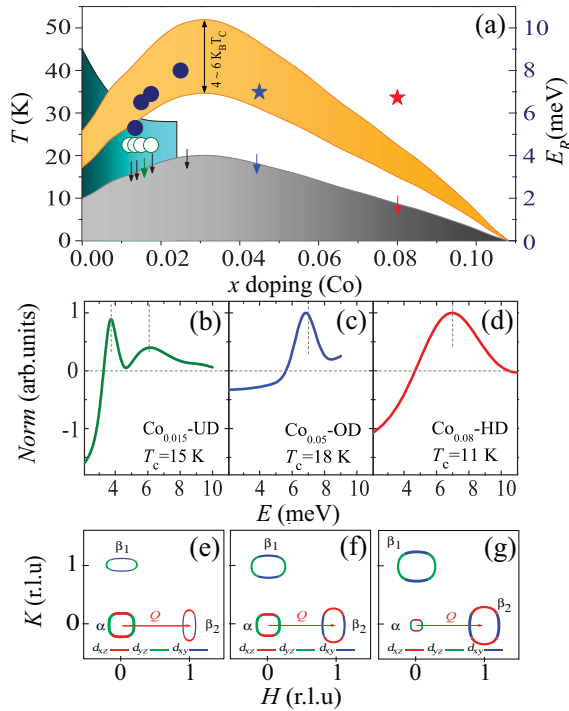
*pdai@rice.edu

FIG. 1. (a) The electronic phase diagram of NaFe$_{1-x}$Co$_x$As, where the arrow indicates the Co-doping levels studied in this paper. The gray shaded area marks the Co-doping dependence of T_c. The region with AF order is represented by the green shaded area. The open circles are energies of the first resonance E_{r1}, and the filled circles and stars are energies of the second resonance E_{r2}. The yellow shaded area indicates approximate range of $E_r \approx 4 - 6k_BT_c$ obtained from previous works [19,20]. (b)–(d) The schematic energy dependence of the resonance for three characteristic Co-doping levels, including underdoped (UD), optimally doped (OD), and highly overdoped (HD). (e)–(g) Schematic plots of the Fermi surfaces for the above three compositions. The color indicate different orbitals. The anisotropic superconducting gap Δ_e on the electron pockets in the underdoped compounds become isotropic on the overdoped side [16].

nor with Δ via $E_r/(\Delta_h + \Delta_e) = 0.64$ [19–21], thus suggesting that the multiorbital character and the interband nonmagnetic impurity scattering due to Co doping in NaFe$_{1-x}$Co$_x$As play an important role in determining the properties of the resonance.

II. EXPERIMENTAL RESULTS

We grew single crystals of NaFe$_{1-x}$Co$_x$As by self-flux method as described before [29]. The sample quality has been characterized by various techniques, which found that bulk superconductivity appears in the doping range of $0.012 \leqslant x \leqslant 0.1$ [15]. Our inelastic neutron scattering experiments were carried out over the entire doping range as shown by vertical arrows in Fig. 1(a). The measurements were performed on the HB-1 and HB-3 thermal triple-axis spectrometers at High Flux Isotope Reactor, Oak Ridge National Laboratory, and SPINS cold triple-axis spectrometer at the NIST Center for Neutron Research. Pyrolytic graphite (PG) monochromator and analyzer were used with fixed final neutron energies at $E_f = 14.7$ meV and $E_f = 5$ meV for thermal and cold neutron measurements, respectively. The corresponding energy reso-
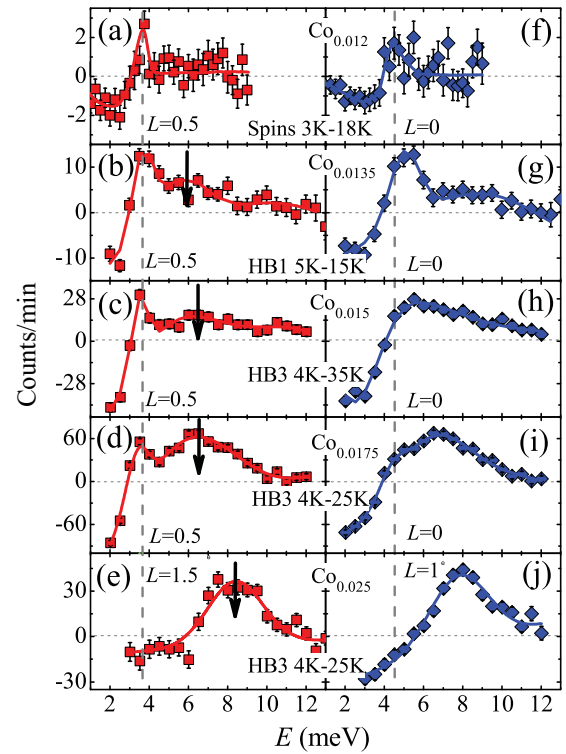

FIG. 2. The neutron resonances in NaFe$_{1-x}$Co$_x$As as a function of increasing x, obtained as the difference of the energy scans above and below T_c at the wave vectors $\mathbf{Q}_{AF} = (1,0,L)$ with $L = 0.5, 1.5$ (a)–(e) and $\mathbf{Q} = (1,0,L)$ with $L = 0, 1$ (f)–(j). (a),(f) $x = 0.012$ (UD); (b),(g) $x = 0.0135$ (UD); (c),(h) $x = 0.015$ (UD); (d),(i) $x = 0.0175$ (UD); (e),(j) $x = 0.025$ (OP). The plots are obtained directly by subtracting the superconducting state energy scan from those in the normal state without correcting for background, as is commonly done for determining the energy of the resonance [3–6]. The solid lines are fits with two Gaussians. The vertical dashed lines denote the low-energy resonance at E_{r1} in (a)–(d) and (f)–(i). The negative intensity below the resonance indicates the opening of a spin gap below T_c. The vertical arrows indicate the peak positions of the high-energy resonance E_{r2} at $\mathbf{Q}_{AF} = (1,0,L)$ with $L = 0.5, 1.5$.

lutions are $\Delta E \approx 1.2$ meV and $\Delta E \approx 0.15$ meV, respectively, at the AF ordering elastic position. Several pieces of crystals coaligned with a total mass of ~ 10 g and the mosaic of $\sim 3°$ were used in each experiment. The wave vector $\mathbf{Q}$ at (q_x, q_y, q_z) in Å^{-1} is defined as $(H, K, L) = (q_x a/2\pi, q_y b/2\pi, q_z c/2\pi)$ in reciprocal lattice unit (r.l.u) using the orthorhombic unit cell where $a \approx b \approx 5.589$ Å and $c \approx 6.980$ Å at 3 K. The samples are aligned in the $[H, 0, L]$ scattering zone, where the resonance occurs at the AF wave vector $\mathbf{Q} = (1,0)$, consistent with the Fermi surface nesting wave vector shown in Fig. 1(e) [27,28]. Some measurements are carried out in the $[H, K, 0]$ scattering plane.

To systematically investigate the electron-doping evolution of the double resonance in the underdoped regime [27], we first focus on a series of compositions from $x = 0.012$ to $x = 0.0175$ [Figs. 2(a)–2(d), 2(f)–2(i)]. Similar to previous neutron scattering work [4,19], we define resonance as the intensity gain of magnetic scattering in the superconducting state. For this purpose, energy scans are carried out at fixed
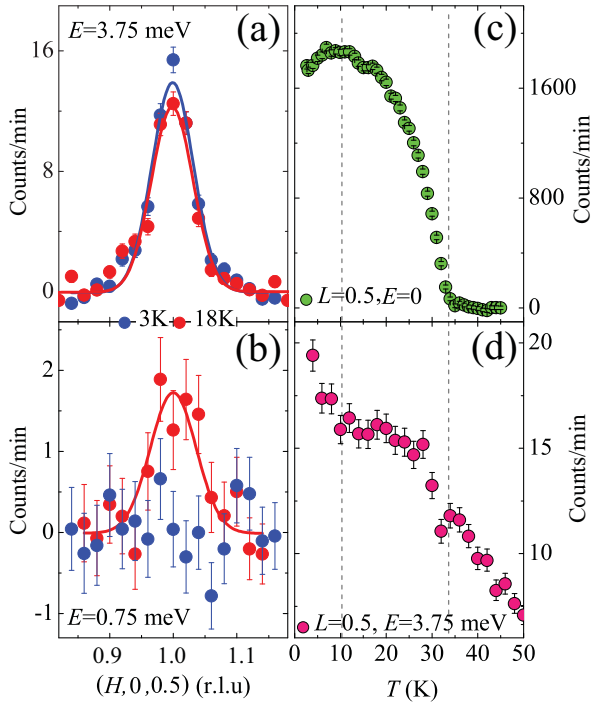
FIG. 3. Wave vector and temperature dependence of the magnetic scattering for NaFe$_{1-x}$Co$_x$As with $x = 0.012$ when the system is near bulk superconductivity. The sample has T_N of $\sim$35 K and $T_c \approx 11$ K. The data was collected on SPINS.
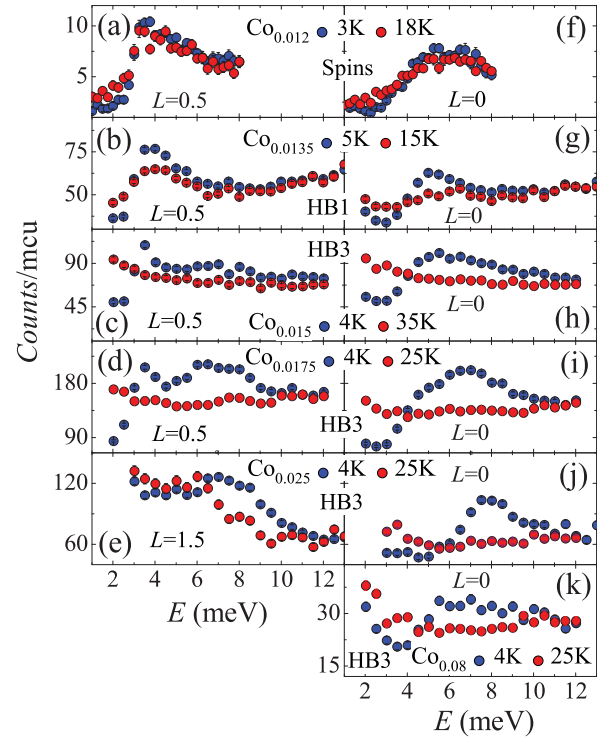

FIG. 4. The raw data of energy scans at wave vectors $\mathbf{Q}_{AF} = (1,0,L)$ with $L = 0.5, 1.5$ (a)–(e) and $L = 0$ (f)–(k) obtained for NaFe$_{1-x}$Co$_x$As with different x above and below T_c.

wave vectors below and above T_c, and the net intensity gain of the scattering below T_c is ascribed to the resonance. In the case of NaFe$_{1-x}$Co$_x$As, previous work has shown that the resonance occurs at slightly different energies at the AF zone center $\mathbf{Q}_{AF} = (1,0,L)$ with $L = 0.5, 1.5$ and zone boundary with $L = 0, 1$ [27]. We have therefore carried out systematic measurements at these two wave vectors for all Co-doping levels. Figures 2(a) and 2(f) show the outcome for NaFe$_{1-x}$Co$_x$As with $x = 0.012$, when the system first becomes near the bulk superconducting phase [15]. The temperature difference plot shows a resonance peak at $E_{r1} = 3.75$ meV for $L = 0.5$ and $E_{r1} = 4.5$ meV for $L = 0$ with the corresponding spin gaps of $E_g \approx 3$ and 4 meV, respectively. To further confirm the existence of the resonance, we carried out momentum and temperature dependence measurements on SPINS. Figure 3(a) shows constant-energy scans at $E_{r1} = 3.75$ meV along the [H,0,0.5] direction, which reveals clear intensity gain below T_c at $\mathbf{Q}_{AF}$. For an energy below the resonance at $E = 0.75$ meV, AF spin fluctuations are completely suppressed below T_c, suggesting the opening of a spin gap in the superconducting state [Fig. 3(b)]. Temperature dependence of the elastic magnetic scattering is shown in Fig. 3(c). Similar to previous work on underdoped superconducting iron pnictides [30,31], we see clear evidence for AF order below $T_N \approx 35$ K and the suppressive effect of superconductivity on AF order. Figure 3(d) shows temperature dependence of scattering at $E_{r1} = 3.75$ meV and $\mathbf{Q}_{AF} = (1,0,0.5)$. Based on these results, we find clear evidence for the resonance in the $x = 0.012$ compound.

At higher doping levels, $x = 0.0135$ [Figs. 2(b) and 2(g)], $x = 0.015$ [Figs. 2(c) and 2(h)], and $x = 0.175$ [Figs. 2(d) and 2(i)], a second resonance mode with a broad width appears at a higher energy E_{r2}. As the superconducting transition temperature T_c increases with increasing Co doping, E_{r2} also increases, whereas E_{r1} stays at almost the same energy for $\mathbf{Q}_{AF} = (1,0,0.5)$. These results suggest that the energy of the first resonance is not directly associated with $k_B T_c$. Furthermore, we note that the spectral weight of the low-energy resonance gradually shifts to the high-energy one with increasing Co doping. Near optimal doping $x = 0.025$ ($T_c = 22$ K) [Figs. 2(e) and 2(j)] [15], the low-energy resonance completely vanishes and only the high-energy resonance is present. Comparing the left and right panels of Fig. 2, we see that in the underdoped regime, the energy of the first resonance shows similar out-of-plane momentum dependence as in the underdoped superconducting BaFe$_2$As$_2$ systems doped with Co, Ni, and P [32], being higher at $L = 0$ than at $L = 0.5$. Near optimal superconductivity, the resonance energy becomes dispersionless, occurring at the same energy for both $L = 0.5$ and 1. Figure 4 shows the raw data below and above T_c for different Co-doping samples obtained at various triple-axis spectrometers. Although energy dependence of the spin excitations spectra are somewhat different in the underdoped samples where superconductivity coexists with static AF order and optimally/overdoped samples where there are no static magnetism, we collected the data below and above T_c to determine accurately the effect of superconductivity on the magnetic excitations spectra.
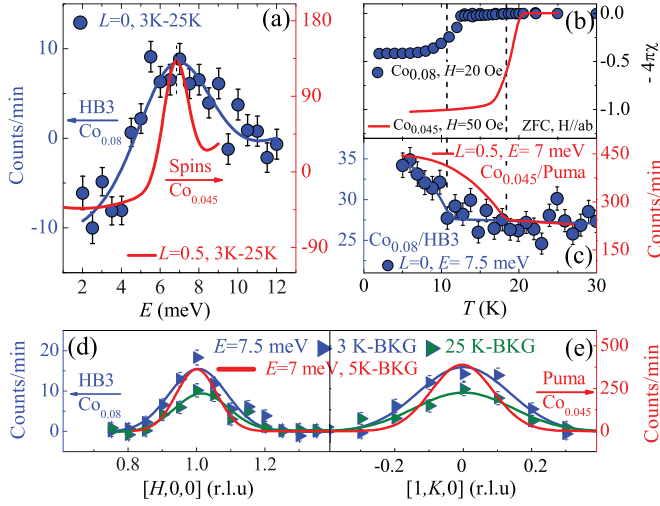
FIG. 5. Comparison of the resonance in the overdoped regime at two compositions $x = 0.045$ and $x = 0.08$. (a) The difference of the energy scans above and below T_c normalized by the corresponding peak intensities. The $x = 0.045$ and $x = 0.08$ compositions have similar peak energies around 7 meV, but have very different energy widths. For Co-doping levels above $x = 0.025$, resonances are not dispersive along the L direction. (b) Temperature dependence of the susceptibility for $x = 0.045$ and $x = 0.08$. The superconducting volume fraction of the $x = 0.08$ sample is about 40%. (c) Temperature dependence of the scattering intensity at the resonance energy, which show the onset of the resonance modes at their respective transition temperatures T_c. (d),(e) The wave vector scans at the resonance energies along the $[H,0,0]$ and $[1,K,0]$ directions below and above T_c for $x = 0.08$. Similar data for $x = 0.045$ at 5 K is shown in red solid line [28]. The blue and green solid lines are Gaussian fits to the data.

Figure 5 summarizes the results for an electron-overdoped sample with $x = 0.08$ ($T_c = 11$ K). Since T_c of the sample is significantly lower than that of the electron doped $x = 0.045$ [Fig. 5(b)] [28], we would expect a reduction in the superconducting gap amplitude $2\Delta = \Delta_h + \Delta_e$ as well [33]. If the resonance is a bound state below the particle-hole continuum 2Δ [5], there should be a corresponding reduction in the mode energy on moving from $x = 0.045$ to $x = 0.08$. Figure 5(a) compares temperature difference plot of the energy scans below and above T_c for $x = 0.045$ to $x = 0.08$. While there is a clear resonance in both samples, the resonance for $x = 0.08$ shows a much broader width compared to that of $x = 0.045$ even considering the differences in instrumental energy resolution in these two experiments. In addition, the two resonances have almost the same peak energy at $E_r = 7$ meV, despite the large reduction in T_c from $x = 0.045$ to $x = 0.08$. To confirm that the intensity gain below T_c in the $x = 0.08$ sample is indeed the resonance, we show in Fig. 5(c) temperature dependence of the scattering at $E_r = 7$ meV. For both $x = 0.045$ to $x = 0.08$ samples, there are clear superconducting order parameter like intensity gain below T_c's, a hallmark of the resonance. Figures 5(d) and 5(e) show constant-energy scans above background below and above T_c along the $[H,0,0]$ and $[1,K,0]$ directions, respectively, for $x = 0.08$. The red solid lines are similar wave vector scans for the $x = 0.045$ sample [28]. These results confirm the
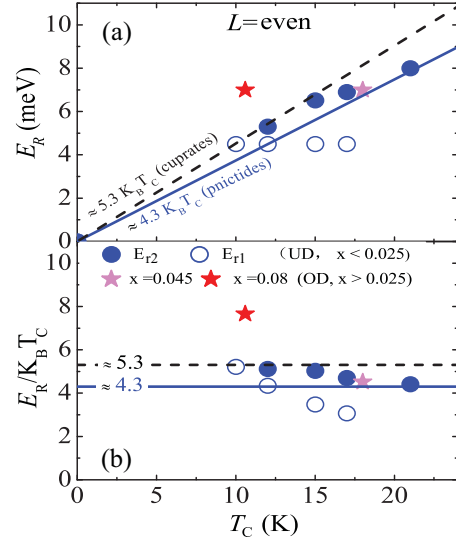

FIG. 6. (a) The Co-doping dependence of the resonance energy E_{r1} and E_{r2} as a function of T_c in NaFe$_{1-x}$Co$_x$As. The solid and dashed lines are expected values for copper oxide and iron pnictide superconductors [20,21]. (b) The ratio E_r/k_BT_c as a function of T_c. The lines represent the expected linear relations. The low-energy resonance E_{r1} in the underdoped regime and the high-energy resonance E_{r2} in the overdoped composition do not follow the expected behavior.

temperature difference plots, showing that intensity gain of below T_c in Figs. 5(a) and 5(c) is indeed from the resonance. Although $x = 0.08$ sample is not a 100% bulk superconductor [Fig. 5(b)], the differences between the superconducting and normal state should still represent the effect of superconductivity to the magnetic excitations. Based on the properties of the resonance in the $x = 0.045$ to $x = 0.08$ samples shown in Fig. 5, we conclude that the mode energy E_r does not scale linearly with T_c or Δ. The ratios E_r/k_BT_c and $E_r/2\Delta$ in the $x = 0.08$ composition are well above the values proposed in the universal relations [see Fig. 1(a)]. Furthermore, we find that while the resonance for both samples are centered at the AF ordering wave vector, the $x = 0.08$ sample has considerable broader **Q** width along the H and K directions.

III. DISCUSSION AND CONCLUSION

Figure 6 summarizes the Co-doping evolution of the resonance in NaFe$_{1-x}$Co$_x$As. The open circles in Fig. 6(a) shows that the energy of the first resonance E_{r1} is essentially T_c independent. If the double resonance originates from the superconducting gap anisotropy in the underdoped regime [16,27,34], one would expect that E_{r1} decreases with increasing doping, contrary to the observation. On the other hand, these results may indicate that the first resonance is coupled with the static AF order and spin waves as suggested theoretically [35]. If this is indeed the case, one would expect that a uniaxial pressure used to detwin the sample would separate the double resonance, where the first resonance associated with spin waves (E_{r1}) should appear at $\mathbf{Q}_{AF} = (\pm 1, 0)$ but not at $(0, \pm 1)$, while the second resonance (E_{r2}) arising from Fermi surface nesting and itinerant electron would

appear at both $\mathbf{Q}_{AF} = (\pm 1,0)$ and $(0,\pm 1)$ wave vectors [36]. However, our recent neutron scattering experiments on the uniaxial pressure detwinned sample found double resonance at both wave vectors, thus suggesting that the first mode cannot be associated with spin waves at $\mathbf{Q}_{AF} = (\pm 1,0)$ [36]. While these results seem to rule out the AF order origin for the first resonance, a more detailed investigation using superconducting gap anisotropy scenario is necessary to determine if such a model can explain our observation [34]. The solid circles and stars in Fig. 6(a) show the T_c dependence of the second resonance energy E_{r2}. While the mode energies for underdoped and slightly overdoped samples fall within the generally accepted values of $E_r \propto k_B T_c$, the resonance energy for $x = 0.08$ clearly deviates from the expectation. Figure 6(b) plots the same data in terms of $E_r/k_B T_c$.

To understand the behavior of the resonance in the electron-overdoped regime of NaFe$_{1-x}$Co$_x$As, we consider two essential effects from Co doping. The first one is the introduction of additional electron charge carriers, which causes the hole pockets to shrink and the electron pockets to expand, as illustrated in Figs. 1(e)–1(g). As the mismatch between the electron and hole pockets increases with doping, the resonance peak obtains more contributions from the scattering momenta that are away from the AF order wave vector (1,0), and therefore shows a broader peak in the momentum space. This is reminiscent of the wave vector dependence of the resonance in BaFe$_{2-x}$Ni$_x$As$_2$ family of materials, where the mode becomes transversely incommensurate in the electron-overdoped regime [37], except here the scattering is commensurate in the entire measured doping range. With electron overdoping and sinking of the hole pocket below Fermi surface, the low-energy spin excitations vanish together with the suppression of superconductivity [38], very similar to the presence of a large spin gap in electron-overdoped nonsuperconducting BaFe$_{1.7}$Ni$_{0.3}$As$_2$ [39]. The

second less considered effect is that the Co dopants can also act as local nonmagnetic impurities. In iron pnictides where the superconducting order parameter changes sign between the hole and electron pockets [Figs. 1(e)–1(g)], interband scatterings from these impurities are superconducting pair breaking. Therefore, as more impurities are introduced with increasing Co doping, we expect the superconducting gap to be gradually filled and the critical temperature T_c to be reduced due to these pair-breaking scatterings. However, the spin resonance arises from the superconducting quasiparticles that retain the original gap amplitude Δ. Therefore, the resonance energy E_r is not much affected by these interband nonmagnetic scatterings, and the mode will acquire a larger width in energy due to the broadened quasiparticle peak with increasing impurity concentration [40]. These results are consistent with our experimental observations, suggesting the important roles of the impurity scatterings in determining the energy and wave vector dependence of the resonance. Our study in the overdoped NaFe$_{1-x}$Co$_x$As have demonstrated that the Co dopants introduce two important effects into the system, namely the additional itinerant electrons and local nonmagnetic impurities.

[1] B. Keimer, S. A. Kivelson, M. R. Norman, S. Uchida, and J. Zaanen, Nature (London) **518**, 179 (2015).

[2] D. J. Scalapino, Rev. Mod. Phys. **84**, 1383 (2012).

[3] P. C. Dai, Rev. Mod. Phys. **87**, 855 (2015).

[4] J. Rossat-Mignod, L. P. Regnault, C. Vettier, P. Bourges, P. Burlet, J. Bossy, J. Y. Henry, and G. Lapertot, Physica C **185**, 86 (1991).

[5] M. Eschrig, Adv. Phys. **55**, 47 (2006).

[6] J. M. Tranquada, G. Xu, and I. A. Zaliznyak, J. Magn. Magn. Mater. **350**, 148 (2014).

[7] P. C. Dai, J. P. Hu, and E. Dagotto, Nat. Phys. **8**, 709 (2012).

[8] A. D. Christianson, E. A. Goremychkin, R. Osborn, S. Rosenkranz, M. D. Lumsden, C. D. Malliakas, I. S. Todorov, H. Claus, D. Y. Chung, M. G. Kanatzidis, R. I. Bewley, and T. Guidi, Nature (London) **456**, 930 (2008).

[9] Y. Kamihara, T. Watanabe, M. Hirano, and H. Hosono, J. Am. Chem. Soc. **130**, 3296 (2008).

[10] G. R. Stewart, Rev. Mod. Phys. **83**, 1589 (2011).

[11] P. J. Hirschfeld, M. M. Korshunov, and I. I. Mazin, Rep. Prog. Phys. **74**, 124508 (2011).

[12] S. L. Li, C. de la Cruz, Q. Huang, G. F. Chen, T.-L. Xia, J. L. Luo, N. L. Wang, and P. C. Dai, Phys. Rev. B **80**, 020504(R) (2009).

[13] Z.-H. Liu, P. Richard, K. Nakayama, G.-F. Chen, S. Dong, J.-B. He, D.-M. Wang, T.-L. Xia, K. Umezawa, T. Kawahara, S. Souma, T. Sato, T. Takahashi, T. Qian, Y. B. Huang, N. Xu, Y. B. Shi, H. Ding, and S.-C. Wang, Phys. Rev. B **84**, 064519 (2011).

[14] S. Thirupathaiah, D. V. Evtushinsky, J. Maletz, V. B. Zabolotnyy, A. A. Kordyuk, T. K. Kim, S. Wurmehl, M. Roslova, I. Morozov, B. Büchner, and S. V. Borisenko, Phys. Rev. B **86**, 214508 (2012).

[15] G. T. Tan, P. Zheng, X. C. Wang, Y. C. Chen, X. T. Zhang, J. L. Luo, T. Netherton, Y. Song, P. C. Dai, C. L. Zhang, and S. L. Li, Phys. Rev. B **87**, 144512 (2013).

[16] Q. Q. Ge, Z. R. Ye, M. Xu, Y. Zhang, J. Jiang, B. P. Xie, Y. Song, C. L. Zhang, P. C. Dai, and D. L. Feng, Phys. Rev. X **3**, 011020 (2013).

[17] M. M. Korshunov and I. Eremin, Phys. Rev. B **78**, 140509(R) (2008).

[18] T. A. Maier, S. Graser, D. J. Scalapino, and P. Hirschfeld, Phys. Rev. B **79**, 134520 (2009).

[19] M. Y. Wang, H. Q. Luo, J. Zhao, C. L. Zhang, M. Wang, K. Marty, S. X. Chi, J. W. Lynn, A. Schneidewind, S. L. Li, and P. C. Dai, Phys. Rev. B **81**, 174524 (2010).

[20] D. S. Inosov, J. T. Park, A. Charnukha, Yuan Li, A. V. Boris, B. Keimer, and V. Hinkov, Phys. Rev. B **83**, 214520 (2011).

[21] G. Yu, Y. Li, E. M. Motoyama, and M. Greven, Nat. Phys. **5**, 873 (2009).

[22] D. R. Parker, M. J. P. Smith, T. Lancaster, A. J. Steele, I. Franke, P. J. Baker, F. L. Pratt, M. J. Pitcher, S. J. Blundell, and S. J. Clarke, Phys. Rev. Lett. **104**, 057007 (2010).

[23] J. D. Wright, T. Lancaster, I. Franke, A. J. Steele, J. S. Möller, M. J. Pitcher, A. J. Corkett, D. R. Parker, D. G. Free, F. L. Pratt, P. J. Baker, S. J. Clarke, and S. J. Blundell, Phys. Rev. B **85**, 054503 (2012).

[24] A. F. Wang, X. G. Luo, Y. J. Yan, J. J. Ying, Z. J. Xiang, G. J. Ye, P. Cheng, Z. Y. Li, W. J. Hu, and X. H. Chen, Phys. Rev. B **85**, 224521 (2012).

[25] A. F. Wang, J. J. Ying, X. G. Luo, Y. J. Yan, D. Y. Liu, Z. J. Xiang, P. Cheng, G. J. Ye, L. J. Zou, Z. Sun, and X. H. Chen, New J. Phys. **15**, 043048 (2013).

[26] G. T. Tan, Y. Song, C. L. Zhang, L. F. Lin, Z. Xu, T. T. Hou, W. Tian, H. B. Cao, S. L. Li, S. P. Feng, and P. C. Dai (unpublished).

[27] C. L. Zhang, R. Yu, Y. X. Su, Y. Song, M. Y. Wang, G. T. Tan, T. Egami, J. A. Fernandez-Baca, E. Faulhaber, Q. Si, and P. C. Dai, Phys. Rev. Lett. **111**, 207002 (2013).

[28] C. L. Zhang *et al.*, Phys. Rev. B **88**, 064504 (2013).

[29] N. Spyrison, M. A. Tanatar, Kyuil Cho, Y. Song, P. C. Dai, C. L. Zhang, and R. Prozorov, Phys. Rev. B **86**, 144528 (2012).

[30] D. K. Pratt, W. Tian, A. Kreyssig, J. L. Zarestky, S. Nandi, N. Ni, S. L. Bud'ko, P. C. Canfield, A. I. Goldman, and R. J. McQueeney, Phys. Rev. Lett. **103**, 087001 (2009).

[31] A. D. Christianson, M. D. Lumsden, S. E. Nagler, G. J. MacDougall, M. A. McGuire, A. S. Sefat, R. Jin, B. C. Sales, and D. Mandrus, Phys. Rev. Lett. **103**, 087002 (2009).

[32] C. H. Lee, P. Steffens, N. Qureshi, M. Nakajima, K. Kihou, A. Iyo, H. Eisaki, and M. Braden, Phys. Rev. Lett. **111**, 167002 (2013).

[33] X. D. Zhou, P. Cai, A. F. Wang, W. Ruan, C. Ye, X. H. Chen, Y. Z. You, Z.-Y. Weng, and Y. Y. Wang, Phys. Rev. Lett. **109**, 037002 (2012).

[34] R. Yu, J. X. Zhu, and Q. Si, Phys. Rev. B **89**, 024509 (2014).

[35] W. C. Lv, A. Moreo, and E. Dagotto, Phys. Rev. B **89**, 104510 (2014).

[36] C. L. Zhang, J. T. Park, X. Y. Lu, R. Yu, Yu Li, W. L. Zhang, Y. Zhao, J. W. Lynn, Q. Si, and P. C. Dai, Phys. Rev. B **91**, 104520 (2015).

[37] H. Q. Luo, Z. Yamani, Y. C. Chen, X. Y. Lu, M. Wang, S. L. Li, T. A. Maier, S. Danilkin, D. T. Adroja, and P. C. Dai, Phys. Rev. B **86**, 024508 (2012).

[38] S. V. Carr, C. L. Zhang, Yu Song, G. T. Tan, Y. Li, D. L. Abernathy, M. B. Stone, G. E. Granroth, T. G. Perring, and Pengcheng Dai, Phys. Rev. B (to be published).

[39] M. Wang, C. L. Zhang, X. Lu, G. Tan, H. Luo, Y. Song, M. Wang, X. Zhang, E. A. Goremychkin, T. G. Perring, T. A. Maier, Z. Yin, K. Haule, G. Kotliar, and P. C. Dai, Nat. Commun. **4**, 2874 (2013).

[40] S. Maiti, J. Knolle, I. Eremin, and A. V. Chubukov, Phys. Rev. B **84**, 144524 (2011).